View metadata, citation and similar papers at core.ac.uk
brought to you by CORE
provided by CiteSeerX

Krypton irradiation damage in Nd-doped zirconolite and perovskite as potential ceramics for inert matrix fuel and plutonium disposition

C. Davoisne[1,2], M. C. Stennett[3], N. C. Hyatt[3], N. Peng[4], C. Jeynes[4] and W. E. Lee[1]

[1] Department of Materials, Imperial College London, London , United Kingdom.
[2] LRCS, CNRS-UMR 6007, Université de Picardie Jules Verne, Amiens, France.
[3] Immobilisation Science Laboratory, Department of Engineering Materials, University of Sheffield, Sheffield, United Kingdom.
[4] Ion Beam Centre, University of Surrey, Guildford, United Kingdom.

Corresponding author: Pr W.E. Lee

Published in Journal of Nuclear Materials **415**(1):67-73 2011

ABSTRACT

Understanding the effect of radiation damage and noble gas accommodation in potential ceramic hosts for plutonium disposition is necessary to evaluate the long-term behaviour during geological disposal. Polycrystalline samples of Nd-doped zirconolite and Nd-doped perovskite were irradiated *ex-situ* with 2 MeV Kr^{+} at a dose of $5x10^{15}$ ions.cm^{-2} to simulate plutonium nuclei recoil during alpha decay. The feasibility of thin section preparation of both pristine and irradiated samples by Focussed Ion Beam sectioning was demonstrated. After irradiation, the Nd-doped zirconolite revealed a well defined amorphous region separated from the pristine material by a thin (40-60 nm) damaged interface. The Nd-doped perovskite contained a defined irradiated region composed of an amorphous region surrounded by damaged regions. In both samples, as revealed by electron diffraction, the damaged regions and interface have a structure in which the fluorite sublattice is present while the pristine lattice is absent. In addition in Nd-doped perovskite, the amorphisation dose depended on crystallographic orientation and possibly sample configuration (thin section and bulk). In Nd-doped perovskite, Electron Energy Loss Spectroscopy study revealed a change in Ti coordination associated with the crystal to amorphous transition.

INTRODUCTION

Civil nuclear and military nuclear programmes generate high level radioactive wastes (HLW). Glasses are widely used for their immobilisation but in the last few decades ceramics have been developed for plutonium disposition and for use as Inert Matrix Fuels (IMF). Candidate ceramics for these applications must fulfil some key requirements which include chemical flexibility to facilitate the incorporation of plutonium and actinides, and good resistance to aqueous dissolution[1][2][3]. Based on these criteria, zirconolite and perovskite are good candidate phases[4][5][6][7] for plutonium disposition.

An understanding of the effect of radiation damage and noble gas accommodation during storage is key to developing a robust safety case. During storage, alpha decay induces formation

of helium and the recoil of the heavy plutonium nuclei induces a high concentration of defects. These result in formation of gas bubbles, defects and voids which can bring about swelling and cracking of ceramic wasteforms. Different approaches have been used to determine the impact of alpha decay; including the study of natural analogues[6][8][9] and *in-situ* ion irradiation of thin sections in a transmission electron microscope (TEM) [4][10][11][12][13]. *Ex-situ* studies, such as reported here, allow simultaneous analysis of pristine and irradiated material by TEM.

In this study, we examined the effect of nuclei recoil in Nd-doped zirconolite and perovskite. The irradiation was performed *ex-situ* using krypton ions. The microstructural and chemical evolution was investigated by TEM, X-ray Energy Dispersive Spectroscopy (EDS) and Electron Energy Loss Spectroscopy (EELS) on thin sections prepared by Focus Ion Beam (FIB).

EXPERIMENTAL PROCEDURE

Irradiations

The samples studied were neodymium doped zirconolite, $(Ca_{0.8}Nd_{0.2})Zr(Ti_{1.8}Al_{0.2})O_7$ and neodymium doped perovskite, $(Ca_{0.9}Nd_{0.1})(Ti_{0.9}Al_{0.1})O_3$. Due to its oxidation state and similar ionic radius to plutonium (Pu^{3+})[14], neodymium was chosen as a surrogate. Ceramics were prepared at the Immobilisation Science Laboratory (the University of Sheffield, Sheffield, UK) as described by Stennett *et al.*[15].

Unlike in *in-situ* irradiation in a TEM during which a specific state of damage is progressively replaced by another, *ex-situ* irradiation followed by FIB preparation of TEM sections enables simultaneous investigation of the different states of damage reproducibly. The main difficulty of this approach, however, is its reliance on determining suitable parameters for *ex-situ* irradiation (energy and fluence). For this study, krypton ions were selected to simulate the plutonium nuclei recoil occurring during alpha decay. Ceramic samples were implanted with krypton ions (2 MeV, normal incidence) at room temperature at the Surrey Ion Beam Centre (the University of Surrey, Guildford, UK) using a 2MV Van de Graaf Implanter. The dose rate was 0.25 μA cm^{-2} and the total dose 5×10^{15} ions cm^{-2}.

The ion range and the number of displacements per atom (dpa) for each ceramic were determined using the Monte Carlo code TRIM[16][17][18] (TRansport of Ions in Matter). The simulation was performed in "Detailed calculation with full damage cascades" mode which gives information about the damage distribution. One of the main parameters for the simulation is the "displacement energy" which corresponds to the necessary energy to eject an atom from its position. Few studies have been undertaken experimentally or using computer simulation to determine this parameter in titanates and zirconates. An energy from 15 to 49 eV was obtained[19][20][21] for oxygen, from 43 to 69 eV[22][21] for titanium, from 25 to 89 eV[22][21] for calcium and 43 eV[21] for zirconium. No displacement energy was reported for neodymium. Considering the range of values for anions and cations reported in these studies, the displacement energies were fixed for all the elements at 50 eV. The calculated results are reported in Table I.

Table I. Average ion range and number of dpa obtained by TRIM calculation

Material	Density (g/cm^3)	Average ion depth (nm)	Straggling (nm)	Maximum number of dpa
Nd-perovskite	4.036	824.4	186.1	5.71
Nd-zirconolite	4.498	789.3	190	5.80

Sample characterisation

Microstructural and chemical characterisation was carried out on JEOL 2000FX operating at 200 keV and FEI Titan 80/300 transmission electron microscopes (TEM). Both microscopes were fitted with Energy Dispersive Spectroscopy (EDS) systems and the sample composition was determined semi-quantitatively using the method developed by Van Cappellen and Doukhan[23] based on the electroneutrality of ionic crystals. The FEI Titan 80/300 is also fitted with a monochromator and a Gatan Tridiem 865 Electron Energy Loss Spectroscopy (EELS) unit allowing an Energy Loss Near Edge Structure (ELNES) investigation on the Ti $L_{3,2}$ edges. Background subtraction considering a power law function and an energy correction with respect to the O K-edge at 530 eV were carried out. As suggested in previous publications[4][24][25], the area and position of the different peaks of the Ti $L_{3,2}$ edges were determined by fitting the spectrum using a specific distribution. In this work, we chose a Voigt (Gaussian-Lorentzian convolution) distribution which is commonly used to fit spectra in e.g. X-ray Photoelectron Spectroscopy (XPS).

TEM sections were prepared by Focussed ion Beam (FIB) sectioning using a FEI FIB200-Secondary Ion Mass Spectrometer (SIMS) with a single gallium beam operating at 30 keV. The FIB was used due to the localisation of the irradiated region (less than 1.5 µm from the sample surface) and the possibility of choosing precisely the region of interest (inside a grain, at a grain boundary). Samples were initially coated with a gold layer (~ 50 nm thick) to avoid charge effects and to protect the surface during imaging. They were then placed into the FIB chamber and a ~ 1µm thick platinum layer, (Figure1a) deposited on the region of interest to protect the surface from damage during milling and imaging. The sample was milled until an electron transparent section was obtained (Figure1.b). Section lift-out was performed *ex-situ* using a micromanipulator and a thin glass needle. The section was attracted and adhered to the tip by the electrostatic effect of the glass needle and transferred to a copper grid with carbon film or holey carbon for imaging in the TEM.

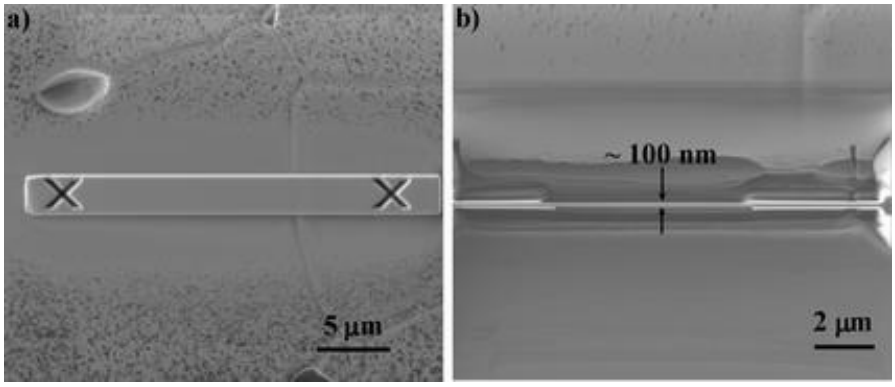

Figure 1. SEM pictures of a TEM section prepared by FIB. a) Platinum deposition on the region of interest in a zirconolite sample and b) perpendicular view of the TEM section after milling (the central part is thinner than the edges).

RESULTS AND DISCUSSION

Pristine sample

Prepared samples of each composition were characterised before irradiation to estimate the damage induced by the gallium beam during the FIB preparation. Considering the TRIM simulation, in the irradiated samples, the damage layer should be located at a depth less than 1.5 µm from the surface. Figure 2 is a view of this region in each sample in which no damage induced by the gallium beam was seen. In some TEM sections, Ga-rich black precipitates are observed, probably arising from precipitation of gallium during milling. Despite the presence of small amounts of gallium in all the sections, the experimental compositions are in good agreement with the theoretical (Table II). Small differences observed are probably due to the sample processing and experimental errors associated with EDS acquisition and spectrum quantification.

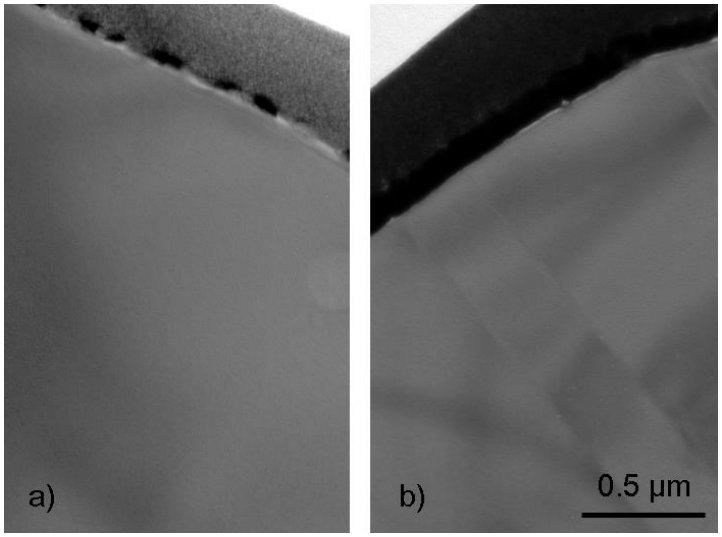

Figure 2. TEM sections after FIB preparation of a) Nd-doped zirconolite and b) Nd-doped perovskite. The scale bar is identical in each.

Sample		O (at%)	Ca (at%)	Ti (at%)	Zr (at%)	Al (at%)	Nd (at%)
Nd-doped perovskite	exp	60.21 ± 0.13	17.24 ± 0.25	18.27 ± 0.46	/	1.73 ± 0.38	2.55 ± 0.21
	th	60	18	18	/	2	2
Irradiated Nd-doped perosvite	exp	60.04 ± 0.48	17.92 ± 1.20	18.12 ± 1.31	/	1.71 ± 0.31	2.22 ± 0.30
Nd-doped zirconolite	exp	63.61 ± 0.12	6.37 ± 0.27	14.38 ± 0.57	11.53 ± 0.57	1.81 ± 0.29	2.00 ± 0.19
	th	63.64	7.27	16.36	9.09	1.82	1.82

Irradiated Nd-doped zirconolite	exp	63.96 ± 0.06	6.33 ± 0.11	14.49 ± 0.43	11.62 ± 0.52	1.87 ± 0.26	1.75 ± 0.27

Table II: Experimental (exp) and theoretical (th) sample composition on pristine and irradiated samples

Kr irradiated samples

In irradiated samples, the presence of a defined damage volume is observed (Figure 3) which extends to a depth of 1.1-1.2 µm for the Nd-doped zirconolite (Figure 3a.) and 0.8-1.1 µm for the Nd-doped perovskite (Figure 3b. and 3c.). These observations are consistent with the TRIM simulation which indicated the damage distribution should extend to approximately 1.2 µm in depth. EDS measurements performed in the irradiated region show no significant deviation from the composition of the pristine samples (Table II).

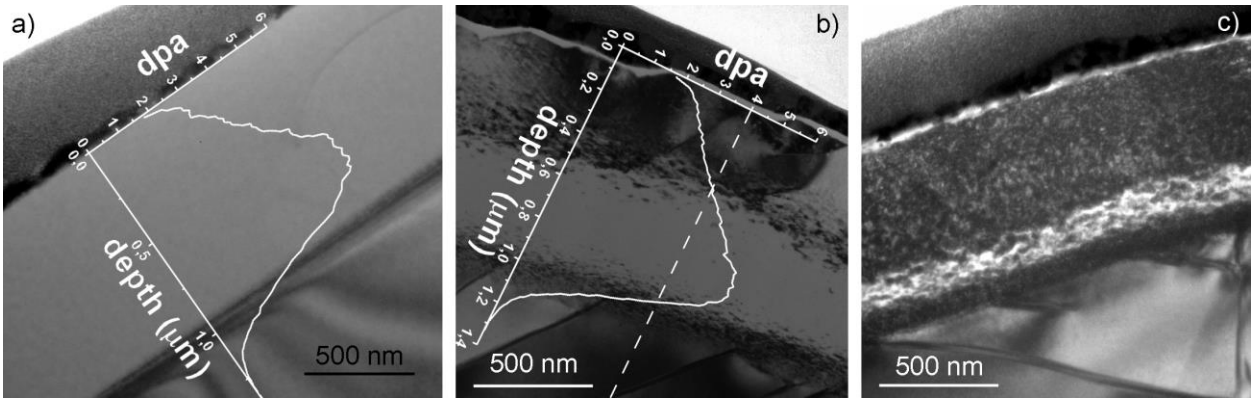

Figure 3.View of the damage region on TEM sections prepared by FIB in Kr irradiated a) Nd-doped zirconolite, b) and c) Nd-doped perovskite. Calculated damage distribution for each composition obtained by TRIM is superimposed in white in a) and b).

In Nd-doped zirconolite, the irradiated region is amorphous as revealed by electron diffraction (Figure 4a). For this material, the amorphisation dose using krypton ions was determined to be ~ 4×10^{14} ions.cm^{-2}[11][8][4]. The presence of an amorphous layer in the sample irradiated at a dose of 5×10^{15} ions.cm^{-2} is therefore consistent with previous studies. For the Nd-doped perovskite, the irradiated region contains an amorphous part (Figure 5C.) comprise between less damaged parts (termed "partly damaged" in the remainder of this paper) (Figure 5B and D). For perovskite, the amorphisation dose using Kr ions has been estimated to be in the range 3.9-18 $\times10^{14}$ ions.cm^{-2} [4][26]. The presence of an amorphous layer in the irradiated region is therefore consistent with previous studies. Figures 3b and c arise from different TEM sections prepared from the same sample on different grains and reveal a greater amorphous volume in Figure 3b than Figure 3c. Considering the entire irradiated region is not amorphous, an estimate of the number of dpa necessary to amorphise the perovskite with Kr^+ ions (2 MeV) can be performed using the correlation between the size of the amorphous region and the TRIM damage distribution. A value of 4 dpa has been estimated considering the damage distribution in Figure 3b. (dotted line). This estimate is higher than the values previously reported during *in-situ* experiments: 1.8 dpa for 800 keV Kr^+ irradiation according Meldrum *et al.*[27][28] and in the

range 0.3-1.5 dpa for 1.5 MeV Kr^{+} irradiation calculated by TRIM according the data from Smith *et al.*[4][26] and a sample thickness of 150 nm (TEM section).

This difference may be due to differences in: i) irradiation conditions (energy, incidence angle), ii) sample configuration (thin section and bulk) and iii) crystallographic orientation of the observed grain. Considering i) irradiation conditions during *in-situ* and *ex-situ* experiments are different in terms of energy (800 keV, 1.5 MeV and 2 MeV) and incidence angle (30° to the vertical and normal incidence). Wang and Ewing[29] have demonstrated the lack of impact of the energy on the amorphisation dose on zircon. The incidence angle will mainly have an impact on the size of the damage distribution. Then, the differences in irradiation conditions cannot explain such difference in the number of dpa necessary to amorphise the sample. For ii) the impact of the sample configuration/thickness on the amorphisation dose has been little studied in the irradiation field and is complicated to approach. Features such as the surface and grain boundaries are sinks for defects especially interstitial atoms which have a higher mobility than vacancies. In a TEM section, the surface to volume ratio is large promoting this type of diffusion. In bulk, this effect is less important and defect recombination is more likely to occur. These differences in defect behaviour can have an impact on the samples evolution under irradiation which is not well known. Defect production must also be taken into account. For *in-situ* experiments[4][26][27][28], considering a classical TEM section (<150 nm thick) and the ion energy and incidence angle, the majority of ions (~92% for energy of 800 keV and ~ 99% for 1.5 MeV) pass through the sample and the damage is mainly induced by recoil atoms. For *ex-situ* experiments, the ions are implanted in the sample and the damage induced by the ions and recoil atoms. The damage maximum is located near the region with the high concentration of implanted ions. This difference of defect production can also have an impact on the microstructural evolution. Considering iii), the different irradiations have been carried out on polycrystalline samples with random crystallographic orientation. In previous studies [30][31][32][33], the existence of crystallographic orientation dependence for damage accumulation during irradiation was demonstrated on various oxides. The anisotropy in damage distribution observed during this study (Figures 3b and c.) can be explained by and reinforces this possibility. All of these differences make it difficult to compare doses and number of dpa necessary to amorphise a sample from one study to another.

A micro-diffraction study was performed to determine the changes due to the irradiation. For the Nd-doped zirconolite, a thorough investigation of the interface between irradiated and pristine regions highlighted the presence of a layer 40-60 nm thick (Figure 4b) whose diffraction patterns indicated a modification in the crystal structure. The change in the relative intensities, the disappearance of the zirconolite superlattice maxima ($h = k = 4n$ and $l = 2m + 1$; $h = k = 4n + 2$ and $l = 2n$) and lines where $h = k = 2n + 1$ is related to a loss of the zirconolite superlattice although the fluorite subcell was retained. In Nd-doped perovskite, the crystal structure is observed to change significantly between the pristine sample and the partly damaged regions. The change in the relative intensities and the disappearance of the perovskite superlattice maxima ($h + l = 2n + 1$ for the following zone axis: [-210], [11-1]; $h + l = 2n + 1$ or $k = 2n + 1$ for [00-1] zone axis) indicate loss of the perovskite superlattice although, as in the zirconolite,

the fluorite subcell was retained. Such microstructural modifications (change in the relative intensities, disappearance of superlattice maxima of the pristine material structure) for zirconolite and perovskite have been reported previously[10][11][12][8][9][4][6] and correspond to a progressive cation disordering induced by the irradiation resulting in the loss of the pristine (zirconolite or perovskite) superlattice while the fluorite lattice remained.

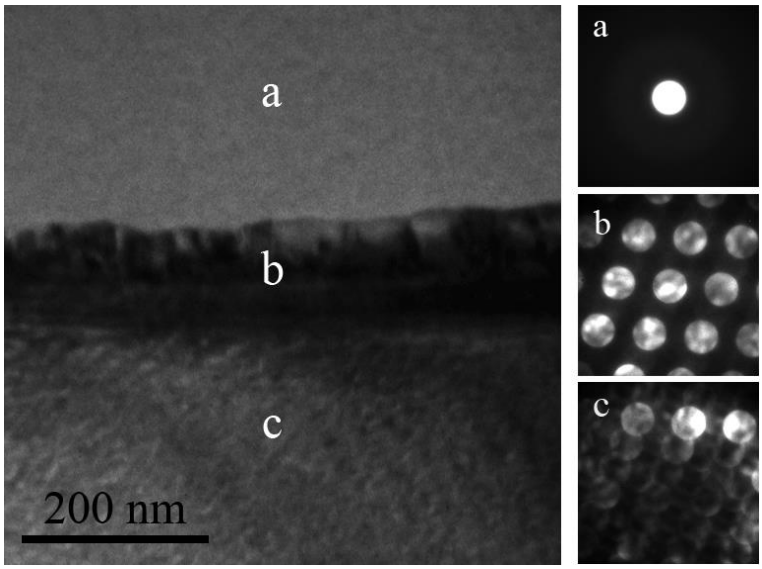

Figure 4. Interface between irradiated and pristine parts of Nd-doped zirconolite. Three regions are visible: a) irradiated region with amorphous diffraction pattern; b) the interphase which remains crystalline but has a different structure from the pristine sample; c) the pristine region which has zirconolite structure, [1-10] zone axis shown.

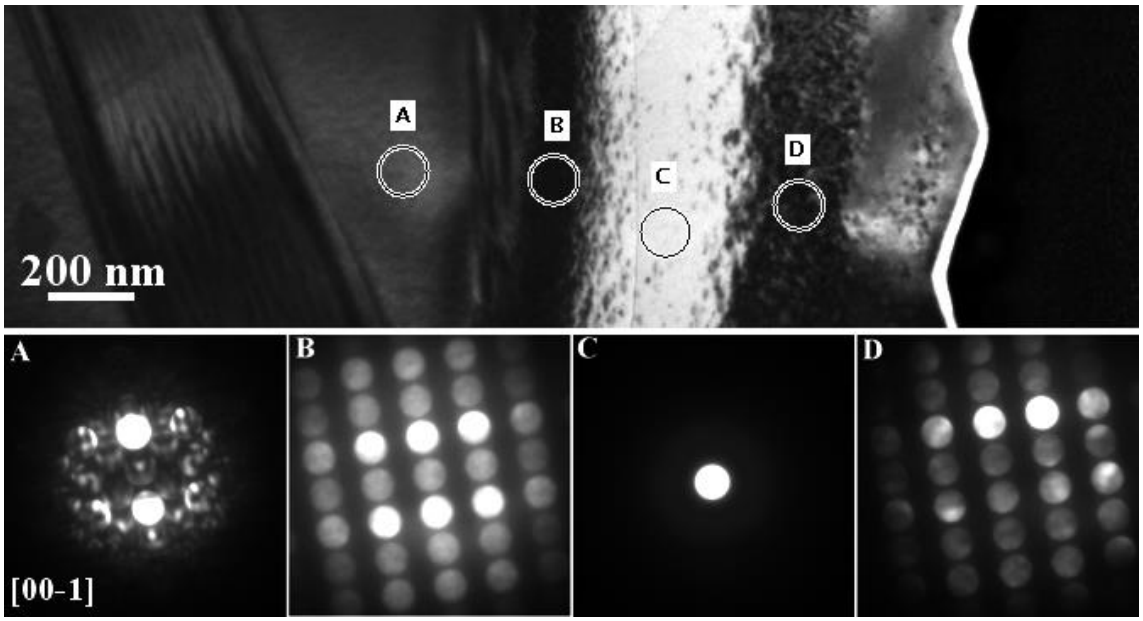

Figure 5. Irradiated and pristine regions of Nd-doped perovskite. Four regions are seen: A) the pristine region which has the perovskite structure, [00-1] zone axis shown; B) and D) a partly

damaged region which remains crystalline but has a different structure from the pristine sample; C) the fully damaged region with amorphous diffraction pattern.

An ELNES study on the Ti $L_{3,2}$ edges of the thinner samples was performed to investigate the change between the pristine and damaged regions. Figure 6b shows a series of spectra taken in the Nd-doped perovskite across the pristine (point analysis 1 in Figure 6a) and irradiated parts (point analysis 2 to 4 in Figure 6a). The peaks labelled L_3 and L_2 correspond to the spin orbit splitting whereas L_3* and L_2* come from molecular orbital splitting [34][35]. The position of the L_3 and L_2 peaks in the pristine region, respectively at 460 and 465.5 eV, is in good agreement with the titanium in the +IV oxidation state [36][37][34][38][35]. Their energy difference is 5.5 eV as reported for TiO_2 by Leapman *et al.*[35]. No change in the position of these peaks is observed in the irradiated region (Figure 6a.). So under irradiation the titanium remains in +IV oxidation state as previously reported in zirconolite[4]. The peaks L_2* and L_3* see their position change and move closer to L_2 and L_3 peaks respectively with the increase of the damage. Figure 6c shows the evolution of the energy difference between L_3-L_3* and L_2-L_2* across the line profile. For both energy differences, a decrease is observed between 0.35 -0.6 µm on the profile which is related to the amorphous region. The decrease in the L-L* energy difference is associated with a change in the titanium coordination number from an octahedral (pristine region) to a tetrahedral (amorphous region) coordination [4][24]. The correlation between the decrease of cation coordination number and amorphisation has been reported previously in studies performed by Extended X-ray Absorption Fine structure (EXAFS) and X-ray Absorption Near Edge Structure (XANES) on similar materials [39][40][41]. No significant change in the L-L* energy difference is observed in the partly damaged regions. This suggests the decrease of the coordination number is only related to the transition from crystalline to amorphous state. Similar results were observed in the Nd-doped zirconolite.

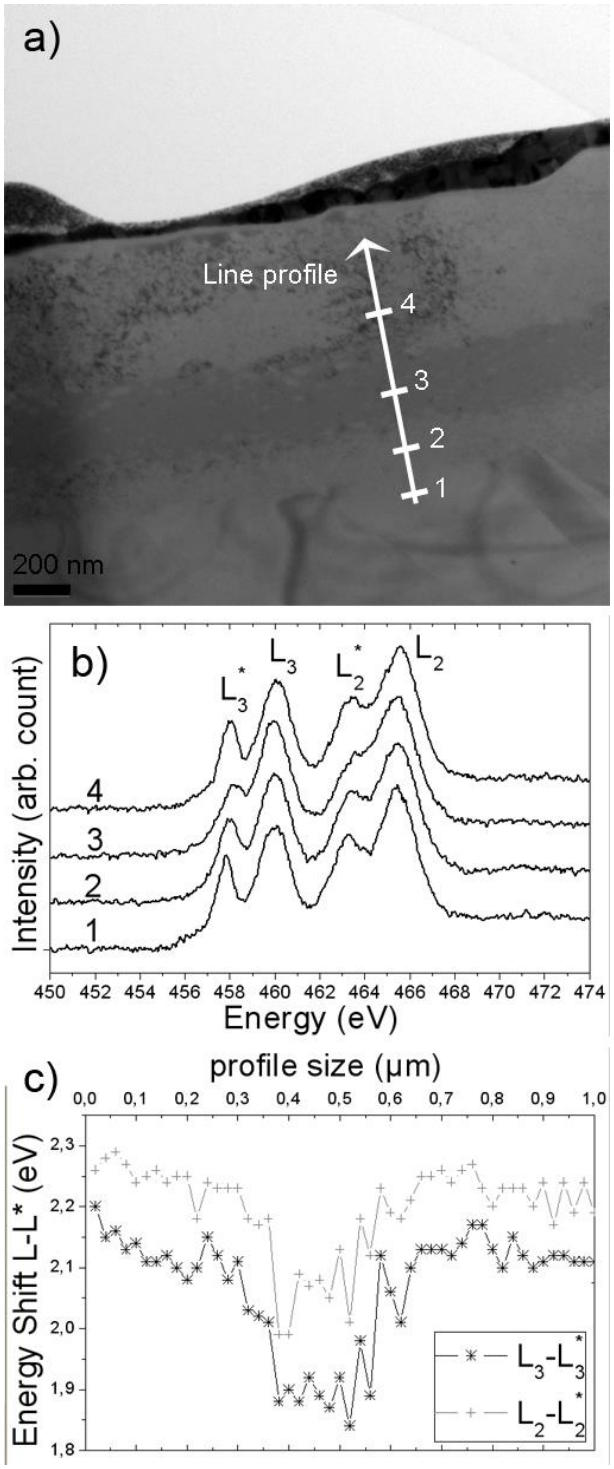

Figure 6.a) Irradiated and pristine parts of the Nd-doped perovskite with the line profile (the arrow indicate the direction of the analysis) and point analysis (1 to 4). b) Spectra of the Ti $L_{3,2}$ edges corresponding respectively to 1 the pristine region, 2 and 4 the partly-damaged regions and 3 the amorphous region. c) Evolution of the L3-L3* and L2-L2* energy difference across the line profile.

CONCLUSIONS

The preparation of TEM sections in pristine and irradiated ceramics such as perovskite and zirconolite by FIB is feasible for examination of specific regions of bulk samples. While artefacts such as gallium precipitates are produced by the ion beam milling process they can be easily identified.

For both Nd-doped zirconolite and Nd-doped perovskite, the structural evolution begins with the loss of the pristine (zirconolite or perovskite) superlattice while the fluorite subcell remained and ends with the samples amorphisation. These modifications are comparable to those observed during *in-situ* TEM irradiation on similar samples.

The amorphisation dose and associated number of dpa are dependent on sample crystallographic orientation and also appear to be sensitive to sample geometry (thin section/bulk) making comparison between *in-situ* and *ex-situ* irradiation experiments difficult.

The EELS analyses on the titanium edge showed no modification in the oxidation state and a decrease in the coordination number. This evolution from an octahedral to a tetrahedral coordination is correlated to the crystal to amorphous transition.

References

[1] R. C. Ewing, Prog. Nucl. Energy 49 (2007) 635-643.

[2] W. E. Lee, M. I. Ojovan, M. C. Stennett, N. C. Hyatt, Adv. Appl. Ceram. 105 (2006) 3-12.

[3] W. J. Weber, R. C. Ewing, C. R. A. Catlow, T. D. de la Rubia, L. W. Hobbs, C. Kinoshita, H. Matzke, A. T. Motta, M. Nastasi, E. K. H. Salje, E. Vance, S. Zinkle, J. Mater. Res. 13 (1998) 1434-1484.

[4] K. L. Smith, N. J. Zaluzec, G. R. Lumpkin, J. Nucl. Mater. 250 (1997) 36-52.

[5] V. M. Oversby, R. A. van Konynenburg, W. E. Glassley, P. G. Curtis, Mater. Res. Soc. Symp. Proc. 333 (1994) 285-292.

[6] W. Sinclair, A. E. Ringwood, Geochem. J. 15 (1981) 229-243.

[7] A. E. Ringwood, S. E. Kesson, N. G. Ware, W. Hibberson, A. Major, Nature 278 (1979) 219-223.

[8] R. C. Ewing, L. M. Wang, Nucl. Instrum. Methods Phys. Res., Sect. B 65 (1992) 319-323.

[9] R. C. Ewing, T. J. Headley, J. Nucl. Mater. 119 (1983) 102-109.

[10] S. X. Wang, G. R. Lumpkin, L. M. Wang, R. C. Ewing, Nucl. Instrum. Methods Phys. Res., Sect. B 166-167 (2000) 293-298.

[11] S. X. Wang, L. M. Wang, R. C. Ewing, G. S. Was, G. R. Lumpkin, Nucl. Instrum. Methods Phys. Res., Sect. B 148 (1999) 704-709.

[12] T. J. White, R. C. Ewing, L. M. Wang, J. S. Forrester, C. Montross, Mater. Res. Soc. Symp. Proc. 353 (1995) 1413-1420.

[13] B. E. Buranov, M. Ojovan, W. E. Lee, Crystalline Materials for Actinide Immobilisation, Imperial College Press, London, UK, 2010.

[14] R. D. Shannon, Acta Crystallogr., Sect. A 32 (1976) 751-767.

[15] M. C. Stennett, N. C. Hyatt, D. Reid, E. Maddrell, N. Peng, C. Jeynes, K. Kirkby, J. Woicik, Mater. Res. Soc. Symp. Proc. 1124 (2009) 243-250.

[16] J. F. Ziegler, J. P. Biersack, M. D. Ziegler, SRIM The Stopping and Range of Ions in Matter, Ion Implantation Technology, USA, 2008.

[17] J. F. Ziegler, Nucl. Instrum. Methods Phys. Res., Sect. B 219 (2004) 1027-1036.
[18] J. F. Ziegler, J. P. Biersack, U. Littmark, The Stopping and Range of Ions in Matter, Pergamon, New york, 1985.
[19] K. L. Smith, M. Colella, R. Cooper, E. R. Vance, J. Nucl. Mater. 321 (2003) 19-28.
[20] R. Cooper, K. L. Smith, M. Colella, E. R. Vance, M. Phillips, J. Nucl. Mater. 289 (2001) 199-203.
[21] L. Veiller, J. -. Crocombette, D. Ghaleb, J. Nucl. Mater. 306 (2002) 61-72.
[22] K. L. Smith, N. J. Zaluzec, J. Nucl. Mater. 336 (2005) 261-266.
[23] E. Van Cappellen, J. C. Doukhan, Ultramicroscopy 53 (1994) 343-349.
[24] R. Brydson, L. A. J. Garvie, A. J. Craven, H. Sauer, F. Hofer, G. Cressey, J. Phys.: Condens. Matter 5 (1993) 9379-9392.
[25] T. I. Morrison, M. B. Brodsky, N. J. Zaluzec, Ultramicroscopy 22 (1987) 125-127.
[26] K. L. Smith, G. R. Lumpkin, M. G. Blackford, E. R. Vance, Mater. Res. Soc. Symp. Proc. 540 (1999) 323-329.
[27] A. Meldrum, L. A. Boatner, W. J. Weber, R. C. Ewing, J. Nucl. Mater. 300 (2002) 242-254.
[28] A. Meldrum, L. A. Boatner, R. C. Ewing, Nucl. Instrum. Methods Phys. Res., Sect. B 141 (1998) 347-352.
[29] L. Wang, R. Ewing, Nucl. Instrum. Methods Phys. Res., Sect. B 65 (1992) 324-329.
[30] I. Usov, P. Arendt, J. Groves, L. Stan, R. DePaula, Nucl. Instrum. Methods Phys. Res., Sect. B 240 (2005) 661-665.
[31] E. Alves, M. F. da Silva, J. C. Soares, T. Monteiro, J. Soares, L. Santos, Nucl. Instrum. Methods Phys. Res., Sect. B 166-167 (2000) 183-187.
[32] G. B. Krefft, E. P. Eernisse, J. Appl. Phys. 49 (1978) 2725-2730.
[33] C. J. McHargue, E. Alves, M. F. da Silva, J. C. Soares, Nucl. Instrum. Methods Phys. Res., Sect. B 148 (1999) 730-734.
[34] R. Brydson, H. Sauer, W. Engel, J. M. Thomass, E. Zeitler, N. Kosugi, H. Kuroda, J. Phys.: Condens. Matter 1 (1989) 797-812.
[35] R. D. Leapman, L. A. Grunes, P. L. FejesS, Phys. Rev. B 26 (1982) 614-635.
[36] E. Stoyanov, F. Langenhorst, G. Steinle-Neumann, Am. Mineral. 92 (2007) 577-586.
[37] G. S. Henderson, X. Liu, M. E. Fleet, Phys. Chem. Miner. 29 (2002) 32-42.
[38] R. Brydson, B. G. Williams, W. Engel, H. Sauer, E. Zeitler, J. M. Thomas, Solid State Commun. 64 (1987) 609-612.
[39] R. Greegor, F. Lytle, R. Livak, F. Clinard Jr, J. Nucl. Mater. 152 (1988) 270-277.
[40] R. Ewing, B. Chakoumakos, G. Lumpkin, T. Murakami, R. Greegor, F. Lytle, Nucl. Instrum. Methods Phys. Res., Sect. B 32 (1988) 487-497.
[41] G. R. Lumpkin, R. C. Ewing, B. C. Chakoumakos, R. B. Greegor, F. W. Lytle, E. M. Foltyn, F. W. Clinard, L. A. Boatner, M. M. Abraham, J. Mater. Res. 1 (1986) 564-576.